1 **Interactions between trade-wind clouds and local forcings**
2 **over the Great Barrier Reef: A case study using convection-**
3 **permitting simulations**

4 Wenhui Zhao[1], Yi Huang[1,2], Steven Siems[2,3], Michael Manton[3], Daniel Harrison[4]

5 [1] School of Geography, Earth and Atmospheric Science, The University of Melbourne, Melbourne, VIC,
6 Australia
7 [2] Australian Research Council (ARC) Centre of Excellence for Climate Extreme (CLEX), Melbourne, VIC,
8 Australia
9 [3] School of Earth, Atmosphere and Environment, Monash University, Melbourne, VIC, Australia
10 [4] National Marine Science Centre, Southern Cross University, Coffs Harbour, NSW, Australia

11 *Correspondence to*: Wenhui Zhao (wenhui.zhao@unimelb.edu.au)

12 **Abstract.** Trade-wind clouds are ubiquitous across the subtropical oceans, including the Great Barrier Reef (GBR),
13 playing an important role in modulating the regional energy budget. These shallow clouds, however, are by their
14 nature sensitive to perturbations in both their thermodynamic environment and microphysical background. In this
15 study, we employ the Weather Research and Forecasting (WRF) model with a convection-permitting
16 configuration at 1 km resolution to examine the sensitivity of the trade-wind clouds to different local forcings
17 over the GBR. A range of local forcings including coastal topography, sea surface temperature (SST), and local
18 aerosol loading is examined.

19 Our simulations show a strong response of cloud fraction and accumulated precipitation to orographic forcing
20 both over the mountains and upwind over the GBR. Orographic lifting and low-level convergence are found to be
21 crucial in explaining the cloud and precipitation features over the coastal mountains downwind of the GBR.
22 However, clouds over the upwind ocean are more strongly constrained by the trade wind inversion, whose
23 properties are, in part, regulated by the coastal topography. On the scales considered in our study, the warm cloud
24 fraction and the ensuant precipitation over the GBR show only a small response to the local SST forcing, with this
25 response being tied to the simulated cloud type. Cloud microphysical properties, including cloud droplet number
26 concentration, liquid water path, and precipitation are sensitive to the changes in atmospheric aerosol population
27 over the GBR. While cloud fraction shows little responses, a slight deepening of the simulated clouds is evident
28 over the upwind region in correspondence to the increased aerosol number concentration. A downwind effect of
29 aerosol loading on simulated cloud and precipitation properties is further noted.

1 Introduction

Trade wind cumuli are ubiquitous across the subtropical oceans (Warren et al., 1988; Norris, 1998; Eastman et al., 2011; Boucher et al., 2013; Rauber et al., 2007), including the Great Barrier Reef (GBR) (Zhao et al., 2022). Despite their limited vertical and horizontal extent, these clouds play a fundamental role in maintaining the thermodynamic budget of the lower troposphere (Chen at al., 2000). These clouds reflect a significant fraction of incoming solar radiation and emit long-wave radiation at relatively high temperature, and thus exert a net cooling effect on the earth atmosphere system (Mumby et al., 2001; Jones et al., 2017). Globally, these clouds help govern earth's energy budget, but are known to be a leading source of uncertainty in future climate projections (Boucher et al., 2013).

The GBR has become increasingly threatened by thermal coral bleaching events (CBEs) over the past decade (Hughes et al., 2017; Stuart-Smith et al., 2018). Recent research has also found that local-scale cloud cover helps regulate the ocean temperature along the GBR with anomalies in the cloud fraction having been directly linked to thermal CBEs (Zhao et al., 2021; Leahy et al., 2013). However, while the large-scale circulation has a fundamental influence on shallow cloud formation, these cloud systems by their nature are sensitive to perturbations in both their thermodynamic environment and microphysical background (Stevens and Brenguier, 2009; Rauber et al., 2007). It is, therefore, important to understand the sensitivity of these low clouds in response to different local forcings.

The GBR contains the world's largest complex collection of coral reefs. It has been hypothesised that the coral reef emissions of dimethylsulfide (DMS) may be an important contributor to the regional atmospheric aerosol loading (Cropp et al., 2018; Fiddes et al., 2021). Any perturbation to the aerosol population would potentially affect the cloud properties and thus the radiative forcing (Lohmann and Feichter, 2005), for instance through a Twomey effect (Twomey, 1997). It has further been hypothesized that the aerosol loading can also affect the precipitation efficiency of these clouds, and thus their lifetime (Cropp et al., 2018; Fischer and Jones, 2012; Deschaseaux et al., 2016; Jones, 2015) through an Albrecht effect (Albrecht, 1989).

Over the GBR, a recent climatology study by Zhao et al. (2022) revealed little to no difference in low-level cloud properties between the open ocean (reef-free region) and the coral reef region, using long-term satellite datasets. These results suggest that low clouds over the GBR do not show a measurable response to the reef-related microphysical perturbations, at least using spaceborne observations. However, subtle signals may be obscured or diminished when averaged over extensive periods in long-term climatological analyses. In addition, a very small natural contribution to the cloud condensation nuclei (CCN) population from coral derived DMS was noted over the GBR (Fiddes et al., 2021). A higher temporal resolution analysis including the diurnal cycle of these low-level clouds may be critical in understanding their effect on the radiation budget. It is, therefore, appropriate to employ high-resolution convection-permitting modelling as an investigation tool to elucidate the full life cycle of these clouds, the development of the precipitation and their response to any perturbations in the aerosol loading (Colle et al., 2005; Smith et al., 2015).

Variations in Sea Surface Temperature (SST), from the shallow water area off the coast to the deeper open ocean and from low to high latitudes over the GBR, could also lead to differences in cloud properties, especially for

67   boundary layer clouds (Crook 1996). SST directly contributes to the thermodynamic conditions, which modulate

68   the sensible and latent heat fluxes, and, consequently, cloud properties such as cloud cover, cloud top height and

69   cloud base (Bony et al., 2004). Significant positive SST anomalies are known to be a key driver of severe thermal

70   coral bleaching periods across the GBR (Berkelmans et al., 2004; Hughes et al., 2017). These large SST anomalies,

71   which could be prevalent for a few months and may spike during periods of weak winds (Filipiak et al., 2012;

72   Gentemann et al., 2003; Zhang et al., 2016), are hence expected to produce a strong local forcing that could change

73   the local thermodynamic conditions.

74   In addition to the aerosol and SST variations, clouds over the GBR can experience other local forcing mechanisms

75   unique to this region. For example, orographic forcing could potentially be important when the south easterly

76   trade winds blow clouds across the Queensland coast and encounter the Great Dividing Range (Houze, 2012).

77   The Wet Tropics of Queensland stretches along the northeast coast of Australia for around 450 km roughly 15-19

78   °S (between the towns of Cairns and Townsville), where significant topography of ~1000m with a peak height of

79   1612 m at Mount Bartle Frere (Sumner and Bonell, 1986) is present. Pronounced precipitation enhancement over

80   the windward slopes of the mountain barrier (Roe, 2005) is commonly observed. The mean annual accumulated

81   rainfall over this large area is among the greatest in Australia (e.g. Bonell and Gilmour, 1980), with the Bellenden

82   Ker Top station receiving over 8000 mm of annual precipitation (Herwitz, 1986) on average. Zhao et al. (2022)

83   found significant orographic enhancement of low-level clouds not only over the Wet Tropics, but also over the

84   upwind ocean extending partially over the GBR. It is therefore of interest to examine any upwind effect of

85   orographic enhancement on shallow cloud and precipitation through high-resolution numerical simulations, where

86   interactions of local variability associated with topography and coastal processes are better resolved.

87   In this paper, we undertake a case study using a series of simulations to explore the sensitivity of trade wind

88   cumulus over the GBR to these different local forcings. In particular, we seek to address three scientific questions:

89   (a) How does the topography of the Great Dividing Range affect the shallow clouds and precipitation over the

90   Wet Tropics including the GBR? (b) Is there any evidence of changes in cloud and precipitation properties in

91   response to SST variations across the GBR? (c) How do the shallow cloud and precipitation properties respond to

92   enhanced local aerosol loading, both over the GBR and downwind over the coast of Queensland? Unlike the study

93   of Fiddes et al. (2021), this study does not aim to test the effects of DMS directly. Rather, it focuses on

94   understanding how strongly, if at all, cloud and precipitation properties respond to changes in the atmospheric

95   aerosol number concentration related to surface emissions. This analysis is also relevant to understanding the

96   integrated effects of potential weather and climate interventions, such as marine cloud brightening, in the heat-

97   sensitive environment of the GBR and its adjacent communities.

98   To address these questions, a range of sensitivity experiments are conducted using convection-permitting

99   numerical simulations. This paper is divided into five sections as follows: Section 2 gives a brief description of

100   the background climate the meteorological conditions of the region, Section 3 details the data and methods used

101   in this study. The main results and discussion are presented in Section 4 and Section 5. Section 6, finally,

102   summarizes the results and provides prospects for future research.

2 29 April 2016 Case Study

The GBR is characterized by a warmer than average monthly sea surface temperature during April 2016 when a thermal coral bleaching event was reported (Zhao et al., 2021). An SST anomaly of over 1°C is identified across much of the GBR (Figure S2), with this SST anomaly being likely to affect the cloud properties, especially low-level clouds through marine atmospheric boundary layer (MABL) processes (Qu et al., 2015; Takahashi et al., 2021). This selected case is characterised by local trade wind cumulus over the Wet Tropics and associated with orographic precipitation on 29th April 2016. This event is also chosen due to the absence of high cloud cover across the Wet Tropics, which are often linked to deeper convection governed by large-scale climate modes such as El Niño-Southern Oscillation (ENSO) and Madden-Julian Oscillation (MJO), as well as the Australian monsoon or tropical cyclones (Tian et al., 2006; Yuan et al., 2013; Eleftheratos et al., 2011; Wu et al., 2012). Note that there is a weak El Niño phase of ENSO during the case study period. Further, the MJO is weak, with the Real-time Multivariate MJO index (Wheeler and Hendon, 2004) less than 1, and no tropical cyclones are recorded across the Northeast Queensland and the GBR.

The mean sea level pressure (MSLP) analysis at 1200UTC of 28th and 29th April 2016 (Figure 1a-b) reveals a Tasman High maintaining the south-easterly trade winds along the northeast coast of Queensland during the case period. Originating in southwest Australia on 22 April, this high-pressure system gradually progressed eastward (not shown). By 26 April, it was positioned over southeast Australia, consequentially producing a high ridge along the northeast coast of Queensland during the following four days. As shown in the Himawari-8 true color images (Figure 1c) at 0000UTC 28th April 2016, northeast Queensland has mostly a clear sky with patches of low-level clouds (stratocumulus, cumulus and stratus, as shown in Figure 1e) extending southwest from the coast in the Wet Tropics. Satellite observations at 0500UTC 29th April 2016 (Figure 1f) reveal a well-developed cloud system consisting of stratocumulus, altocumulus and altostratus. Orographic precipitation associated with trade wind cumuli is captured by land-based rain gauges at several weather stations (Figure 2) on 29th April. The heaviest precipitation was recorded over the eastern slopes and mountain peaks, which is expected under the influence of upslope lifting under the prevailing southeasterly wind regime. From 0600UTC 30th April, the cloud system over the Wet Tropics started dissipating, as observed by satellite images (not shown).
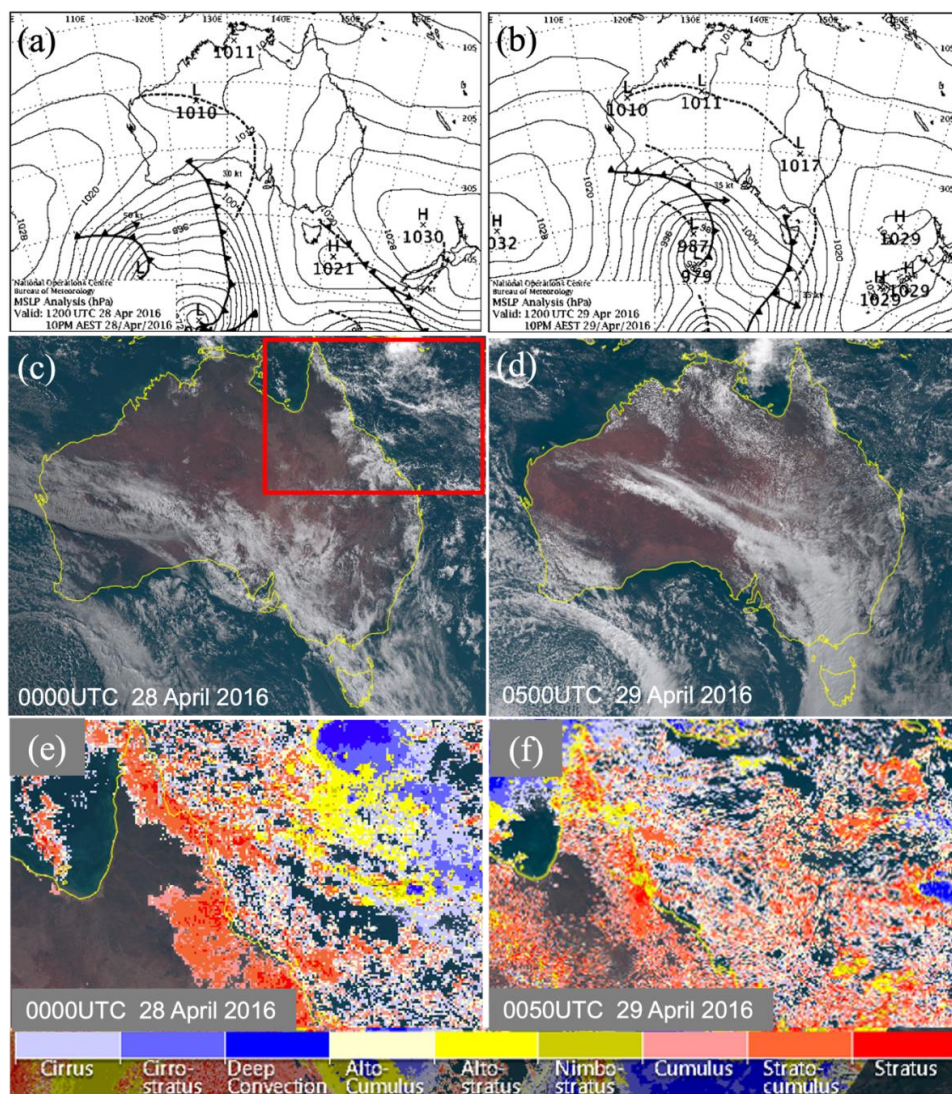
Figure 1: Mean Sea-Level Pressure (MSLP) analyses for 2016 April case at (a) 1200UTC 28th and (b) 1200UTC 29th. Himawari-8 true color imagery for (c) 0000UTC on 28th April and (d) 0500UTC on 29th April 2016. Himawari-8 cloud type classification for (e) 0000UTC on 28th April and (f) 0500UTC on 29th April 2016 for the domain shown by red rectangle in (c). Cloud types as listed on the colorbar for (e-f) are Cirrus, Cirrostratus, Deep Convection, Altocumulus, Altostratus, Nimbostratus, Cumulus, Stratocumulus, and Stratus. Images (a-b) are provided by the Australian Bureau of Meteorology. Images (c-f) are supplied by the P-Tree System, Japan Aerospace Exploration Agency (JAXA).
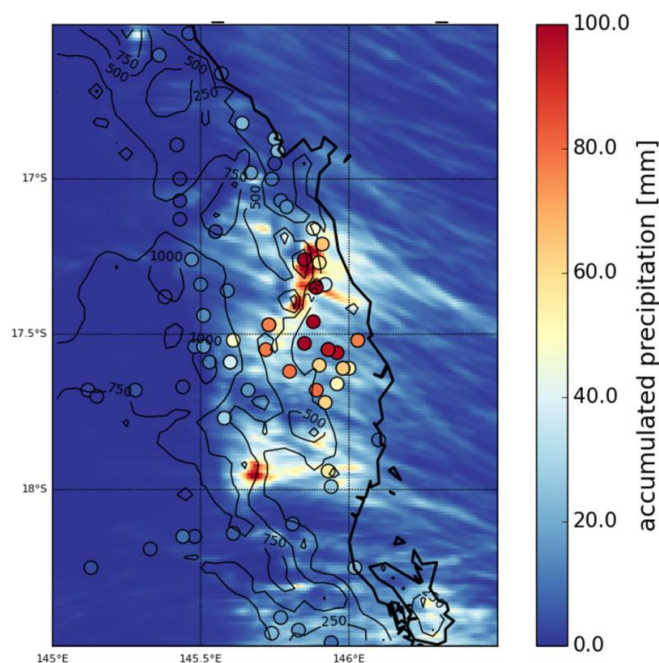
Figure 2: The 48-h accumulated simulated precipitation amounts from 1km resolution with CTRL from 2016-04-27 23:00UTC to 2016-04-29 23:00 UTC overlaid with the precipitation observed by rain gauges shown as filled circles using the same color scale. Black contours indicate the topography map from 250 to 1500 m by 250 m-interval.

3 Data and Methodology

3.1 Model configuration

The Weather Research and Forecasting (WRF, version 4.2; Skamarock et al., 2019) model is used to simulate the interactions between trade wind cumulus and local forcings. In this study, the model is configured with unevenly distributed 65 levels in the vertical, allowing for 30 levels in the lowest 3 km where most of the trade cumulus clouds reside. Three nested domains with horizontal grid spacing of 9km, 3km, and 1km are utilized (Figure 3a). The innermost domain (d03) is set up with 562×457 grid points covering most of the significant topography over the Wet Tropics, extending over the GBR. The model uses the fifth-generation atmospheric reanalysis (hourly, $0.25° \times 0.25°$ grid, 37 set pressure levels and surface level) from the European Centre for Medium Range Weather Forecast (ERA5 reanalysis, Hersbach et al., 2018; 2020) for initial and lateral boundary conditions, as part of the standard WRF pre-processing system (WPS). The control (CTRL) simulation is initialized at 1200UTC 27 April 2016 and run for three days (i.e. 72 hours) with the first 12 hours being used as the spin-up time. It is worth noting that sensitivity to different spin-up times (e.g. 12h, 18h, and 24h) has been tested, and the simulation with a shorter spin-up time (12h) produces a better agreement with observations for this case (not shown).
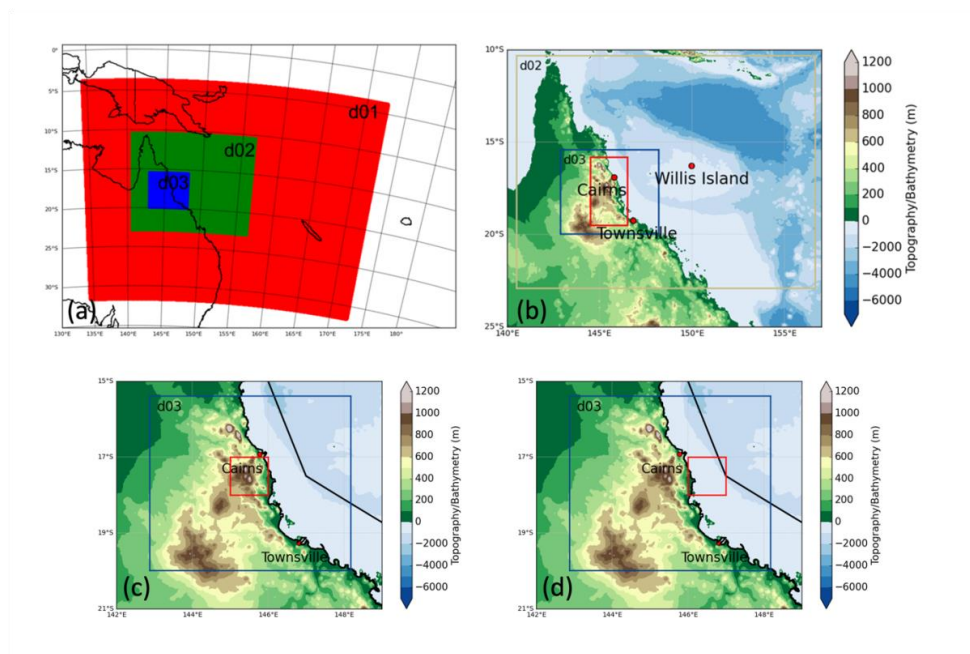
Figure 3: (a) The WRF three nested domains shown by different color boxes used in this study. (b) Zoomed-in topographic-bathymetric map of the two inner domains (shown by colored rectangles) with the locations of two sounding stations (Townsville and Wills Island). The solid red rectangle points out the location of the Wet Tropics. Black lines indicate the GBR general reference map. (c) 1° × 1° downwind sub-domain shown by red rectangles. (d) same as (c), but for upwind sub-domain

The history intervals of prediction outputs are set to be 6h for d01, 3h for d02, and 1h for d03. Simulations are performed with the Yonsei University (YSU, Hong et al., 2006, first-order nonlocal) planetary boundary layer (PBL) scheme, "Noah" land surface model (Chen and Dudhia, 2001), and the RRTMG (Mlawer et al., 1997) scheme for shortwave and longwave radiation, respectively. The same schemes are used for each domain, with the exception of the cumulus scheme. The Kain-Fritsch (Janjić 2000) cumulus parameterization is used only for the coarsest domain (d01) to represent sub-grid convection. For the microphysical parameterization, the Thompson Aerosol Aware microphysics scheme (Thompson and Eidhammer, 2014) is used. Rather than assuming all model horizontal grid points have the same vertical profiles of cloud condensation nuclei (CCN) and ice nucleating (IN) aerosols, this study uses an auxiliary aerosol climatology as the aerosol background condition placed into WRF model. The aerosol input data are derived from multiyear (2001-2007) global model simulations (Calarco et al. 2010). This scheme incorporates the activation of aerosols as CCN and IN, which is determined by a lookup table that employs the simulated temperature, vertical velocity, number of available aerosols, and hygroscopicity parameter applied in Köhler activation theory. Rather than considering multiple aerosol categories, this scheme simply refers to the hygroscopic aerosol as a "water friendly" aerosol and the nonhygroscopic ice-nucleating aerosol as "ice friendly". The activation of aerosols as droplets is done at cloud base as well as anywhere inside a cloud where the lookup table value is greater than the existing droplet number concentration (Thompson and Eidhammer, 2014). The Thompson Aerosol Aware scheme has been shown in previous studies

177   to have promising skill in representing both supercooled and warm liquid conditions of grid-scale clouds (Weston
178   et al., 2022; Wilkinson et al., 2013).

179   An overview of the parameterization schemes used in the CTRL simulation is provided in Table 1. It is worth
180   noting that other configurations with different microphysics, boundary layer, and cumulus schemes have also been
181   tested, and the simulation with the configuration listed in Table 1 is found to be most skilful when evaluated
182   against observations. This configuration is therefore used as our CTRL run and the same configuration settings
183   are applied to all sensitivity experiments.

184   **Table 1: A list of configuration settings for numerical study**

Parameterisation	Option No. (d01, d02, d03)	Comments
Microphysics	mp_physics = 28	Thompson Aerosol Aware (2014) scheme
PBL	bl_pbl_physics = 1	YSU PBL scheme
Cumulus	cu_physics = 1 (d01 only)	Kain-Fritsch scheme (d01 only)
Land/Sea surface	sf_surface_physics = 2	Noah Land Surface Model
Short wave radiation	ra_sw_physics = 4	RRTMG shortwave
Long wave radiation	ra_lw_physics = 4	RRTMG scheme

185

186   **3.2 Sensitivity experiments**

187   Five sensitivity experiments are undertaken to examine the impacts of various local forcings, as detailed below:

188   In the topography experiment, the orography above 300 m is reduced by 75% (Figure S1), named 'Topo300', as
189   similarly done in Flesh and Reuter (2012) and Sarmadi et al. (2019). A threshold of 300m is chosen because it is
190   approximately the mean altitude of the Wet Tropics region, hence representing the background geography. A 75%
191   reduction is used in order to preserve some of the topographic features, and to avoid drastic changes of topography
192   that may induce dramatic changes in the larger-scale circulations. We note that a 500 m threshold is also tested
193   and yielded similar results (not shown).

194   For the local SST forcing, two sensitivity simulations have been conducted in which the monthly mean
195   climatological SST condition for April (namely 'SST-climatology', Figure S2) and 1°C cooler than real SST
196   condition (namely 'SST-cooler') are used to initialize the simulation. SST modifications are applied to the whole
197   ocean area for all three domains. It should be noted that, as with CTRL, the SST conditions are fixed through the
198   3-day simulations.

199   Finally, the climatological surface water-friendly aerosol (WFA) emissions (kg^{-1} s^{-1}) over the GBR (see general
200   reference map in Figure 3b) is increased by a factor of 2 and 5, respectively, to test the sensitivity of warm cloud
201   and precipitation to the aerosol loading to emulate a scenario of enhanced aerosol population associated with coral
202   reef emissions (named 'Aerosol2' and 'Aerosol5', respectively, Figure S3).

203 Table 2 summarizes the details of these sensitivity experiments.

204 **Table 2: Detailed information of numerical experiments conducted in this study.**

		Modification description
CTRL-run		N/A
Sensitivity experiments	Topo300	Decreases elevation by 75% for elevations above 300m
	Aerosol2	Climatological surface WFA emissions increased by 200%, GBR only
	Aerosol5	Climatological surface WFA emissions increased by 500%, GBR only
	SST-cooler	SST reduced by 1°C, whole ocean domain
	SST-climatology	SST replaced by 21-yr (from 1998 to 2018) April climatology, whole ocean domain

205

206 **3.3 Observational Data**

207 Several observational datasets and reanalysis are used to evaluate the simulation across a range of spatial-temporal

208 scales. In this study, sounding data at 0000 UTC and 1200UTC during the simulation period are obtained from

209 the University of Wyoming upper-air sounding database for two selected radiosonde stations (Townsville, code:

210 94294 and Willis Island, code: 94299). To evaluate the large-scale meteorological background conditions in the

211 simulation, hourly mean sea level pressure (MSLP) and wind field at 10 m are also obtained from ERA5 reanalysis

212 with a resolution of 0.25° for the case period (Hersbach et al., 2020). It is worth noting that the simulated synoptic

213 conditions are reasonably consistent with ERA5, although this is largely expected as the simulations are initialized

214 with ERA5 reanalysis in this study. Channel 13 brightness temperatures from the Himawari-8 satellite dataset

215 (Bureau of Meteorology, 2021) and daily rainfall datasets from continuous weather stations are obtained from the

216 Australian Bureau of Meteorology for the case study period. A total of 60 stations are selected, and their spatial

217 distribution is shown in Figure 6.

218 **3.4 Identifying the trade wind inversion**

219 The trade wind inversion (TWI), which results from the interaction of large-scale subsiding air from the upper

220 troposphere and rising air from lower levels that is driven by convection, plays an important role in defining cloud

221 structure and vertical development (Riehl et al., 1979; Albrecht, 1984). Under a trade-wind regime, the top of a

222 cloud layer typically marks the base of the inversion.

223 In this study, we use the same criteria identified in Murphy et al. (2017) to examine the TWI characteristics and

224 its interaction with clouds. Four variables are used: (1) pressure, (2) height, (3) dry bulb temperature, and (4)

225 relative humidity. The criteria used are as follows:

226 a) The TWI is restricted to the 850-600 hPa layer and environmental temperatures greater than 273 K.

227 b) The base of the TWI is defined where the temperature begins to increase, and relative humidity decreases

228 with height.

229 c) The top of the TWI is defined by a vertical temperature decrease with height.

230   d) When multiple inversions are detected, the layer with the greatest relative humidity decrease is selected
231   as the TWI.

232 Two properties, in addition to the inversion base height, describing the TWI are defined also following the method
233 described in Murphy et al. (2017). The inversion thickness (km) is the difference in height between the base and
234 top of the inversion, while the inversion strength or magnitude (K) is the temperature increase across the inversion.

235 **4 Control simulation**

236 In this section, the simulated synoptic and the surface features are first evaluated by comparing the results of the
237 control simulation with observations. It is found that the control simulation skilfully simulated the evolution of
238 the large-scale synoptic patterns of the MSLP in terms of both the progression and the magnitude of the surface
239 pressure system (not shown). Simulated wind conditions at 850 hPa at 0000 UTC 28 April (the first hour after
240 spin-up time) are compared with ERA5 reanalysis, and the 3 km WRF simulated pattern and magnitude of the
241 wind field are found to be generally in good agreement with the reanalysis (Figure 4). Good agreement is also
242 found towards the end of the simulation (1200UTC 30 April), with both wind speed and direction agreeing
243 reasonably well with the reanalysis (Figure 4). Figure 5 shows the observed soundings (black) from the two
244 available sounding stations (Willis Island and Townsville) within the domain and the simulated atmospheric
245 profile (red) at the nearest grid point in the 3 km domain at 0000 UTC on 28 and 30 April. The simulated soundings
246 at the two sites both have good agreement with observations at the beginning and the last day of the simulation,
247 with both wind speed and direction well captured throughout the profile. The simulation accurately predicts the
248 cloud base height (around 850 m) and surface temperature at the two sites, and it is worth noting that the wind
249 inversion at 800 hPa at Townsville station is well captured throughout the simulation (Figure 5).

250 Figure 5 compares the observed and simulated brightness temperature throughout the simulation period. Note that
251 the simulated brightness temperature is simply calculated assuming an emissivity of one for all surfaces and an
252 effective cloud optical depth of one. It is used for a qualitative evaluation of the simulated cloud field only. Overall,
253 the cloud field is reasonably well simulated in terms of the location and timing when compared against the
254 Himawari-8 observation. Although the chaotic nature of shallow cumulus cloud means that details are not fully
255 aligned, the major cumulus cloud features over the Wet Tropics throughout the three-day simulation period has
256 been well captured.

257 Figure 2 shows the 48 h accumulated precipitation from the 1 km WRF simulation, overlaid with the observed
258 rainfall shown as filled circles using the same color scale. The orographic signature (see Figure 3b and black
259 contours in Figure 6), as shown in the correlation between the accumulated precipitation amounts and topography,
260 is evident in both the observed and simulated precipitation. The overall distribution of the simulated accumulated
261 precipitation shows a good agreement with the rain gauge observations, with the majority of the precipitation
262 produced over the windward side of the topography. Although a bias is noted in the location of the peak
263 precipitation, the simulated accumulated precipitation amounts agrees reasonably well with the rain gauge
264 observations.
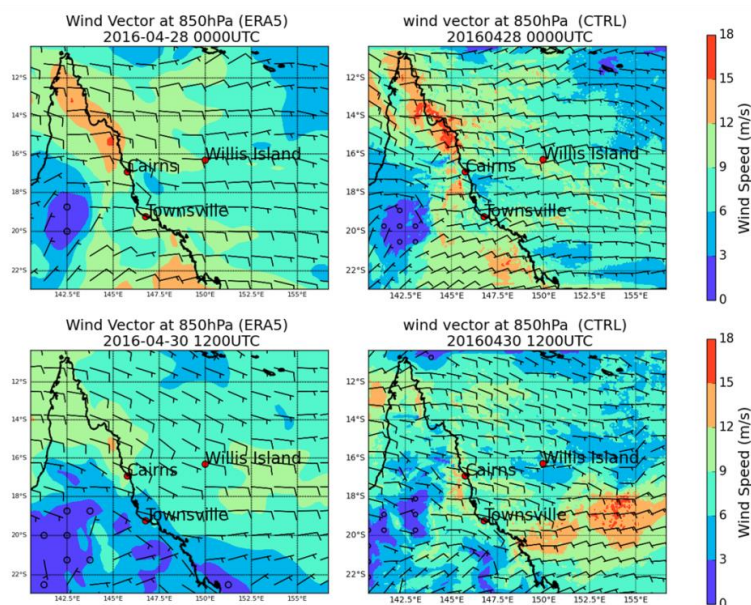
Figure 4: Wind vector distribution at 850 hPa from (left) ERA5 and (right) WRF simulations from CTRL-run at 0000UTC 28th and 1200UTC 30th April 2016. Note that same color scales are applied in all panels.
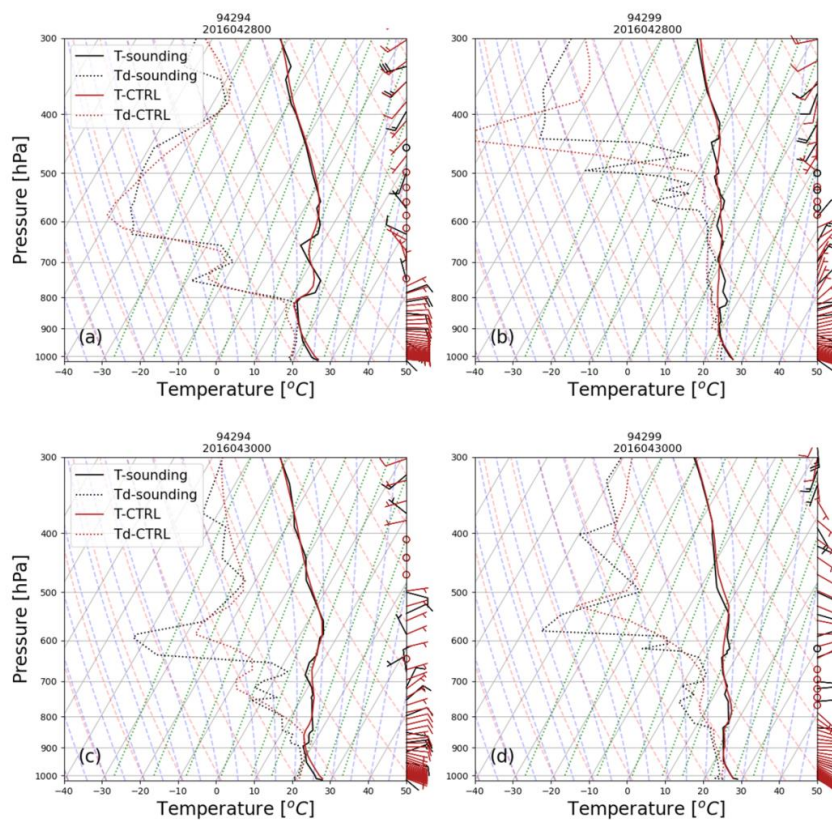
Figure 5: Comparison of the observed upper air soundings (black lines) from (a) Townsville and (b) Willis Island alongside 3 km WRF simulations (red lines) from the nearest grid point to two stations on 28 of April 2016 at 0000 UTC. (c-d) same as (a-b), but for the time of 0000UTC on 30 April 2016.

272
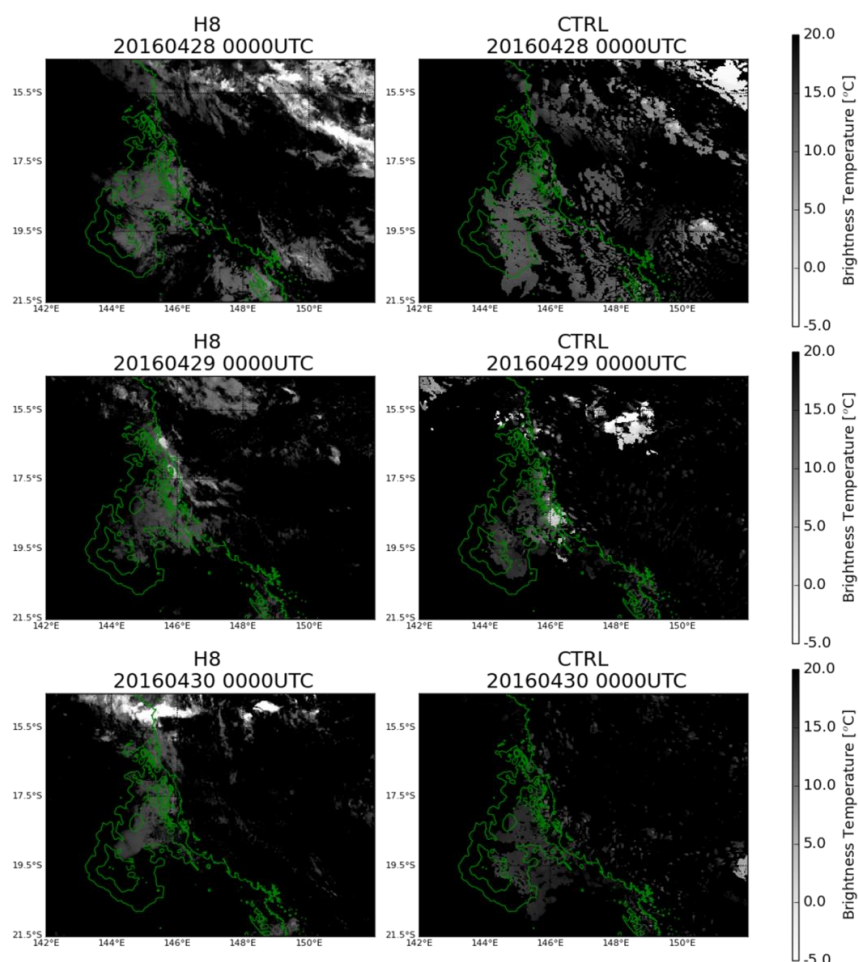
Figure 6: (left) Brightness temperatures of band 13 (10.4 μm) derived from Himawari-8 satellite observations at 0000UTC on 28, 29 and 30 April 2016. (right) Simulated brightness temperatures from CTRL at 3 km resolution at 0000UTC on 28, 29 and 30 April 2016. Note that same color scales applied in all panels. Green lines denote the coastline and topography map from 500 to 1500 m with 250 m interval.

277

5 Sensitivity analysis

5.1 Orographic effects

To explore any upwind effect of the orography over the Wet Tropics, two 1° x 1° sub-domains are selected with one covering the primary orographic area (hereafter downwind sub-domain, Figure 3c) where the major precipitation occurs (see Figure 2 and Figure 9a), and another over the upwind water area (hereafter upwind sub-domain, Figure 3d). The simulated cloud fraction (CF) has been analysed over these two sub-domains,

284 respectively. In this study, CF is defined as the proportion of total grid points in the target domain that are classified

285 as cloudy grids, denoted by the binary number 1, for each model level. For each model level from 0.5 to 6 km, the

286 CF is calculated for each hour. Figures 7 and 8 show the 2-dimensional Probability Density Function (PDF)

287 distribution of the CF across the domains for the 60 hours of simulation. To generate the PDF, 100 bins are applied

288 to both variables CF and altitude. Then the probability density for each grid point is calculated based on CF

289 samples at model levels from 60 simulations hours. The uppermost level of this analysis is set to 6 km as most of

290 the clouds are observed to be at low to mid-level during the simulation period. As shown in Figure 7a and 8a, the

291 simulated CF over these sub-domains from CTRL is between 0.5 and 2.5 km (i.e. boundary layer clouds and trade

292 wind cumuli). Note that the boundary layer height over the Wet Tropics is around 950 m in the CTRL run (not

293 shown) and the trade wind inversion base is at around 2 km (see Figure 10a).

294 Comparing the simulated CF distribution between Topo300 and CTRL runs over the orographic area (Figure 7d),

295 there appears to be a noticeable decrease in cloud cover in the Topo300. The most pronounced reduction is evident

296 at lower altitudes, specifically below 2 km. Cloud top height is generally reduced in Topo300, with a greater

297 number of simulation hours in Topo300 indicating a CF near zero above 2km. This same feature is also seen over

298 the upwind coral reef area (Figure 8d), though the magnitude of the CF is relatively small compared to the

299 mountain area. Larger differences in CF are, once again, found at lower altitudes (below 2 km). It is interesting to

300 note that the orographic enhancement of the low-level cloud fraction, extending to the eastern water area,

301 potentially provides a sheltered area for the coral reefs, protecting them from severe bleaching through reducing

302 the solar radiation heating. This result is consistent with the observational analysis presented by Zhao et al. (2022),

303 which highlighted a notable increase in the frequency of low-level clouds associated with orographic enhancement

304 in the Wet Tropics.
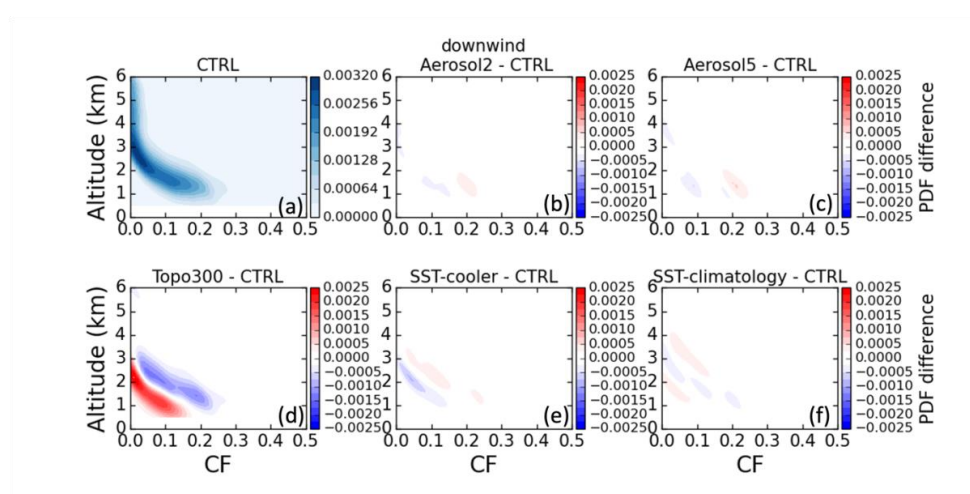
305

306 **Figure 7: (a) Vertical PDF distribution of 1 km resolution simulated cloud fraction over the downwind mountain area**

307 **(shown by red square in Figure 3c) from CTRL-run. (b-f) Difference plots between CTRL-run and Aerosol2, Aerosol5,**

308 **Topo300, SST-cooler, SST-climatology. The analysis is for 60h simulation time after the spin-up from 2016-04-28**

309 **0000UTC to 2016-04-30 1200UTC.**
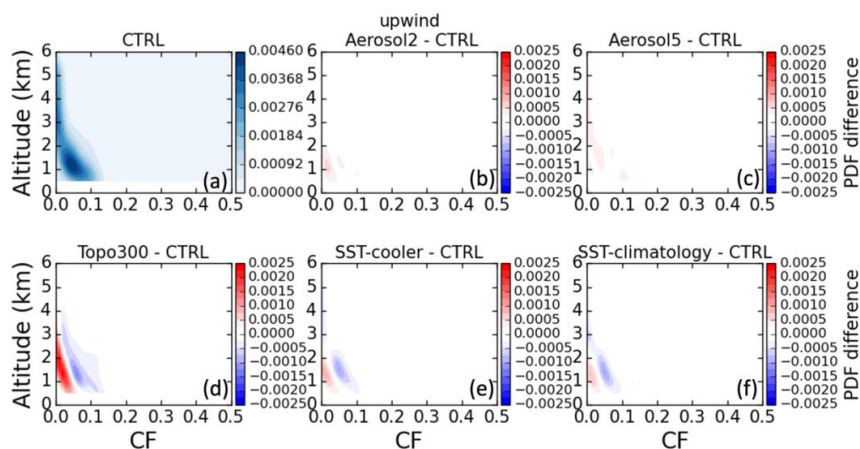
310

311 **Figure 8: Same as Figure 7, but for the upwind water area (shown by red square in Figure 3d).**
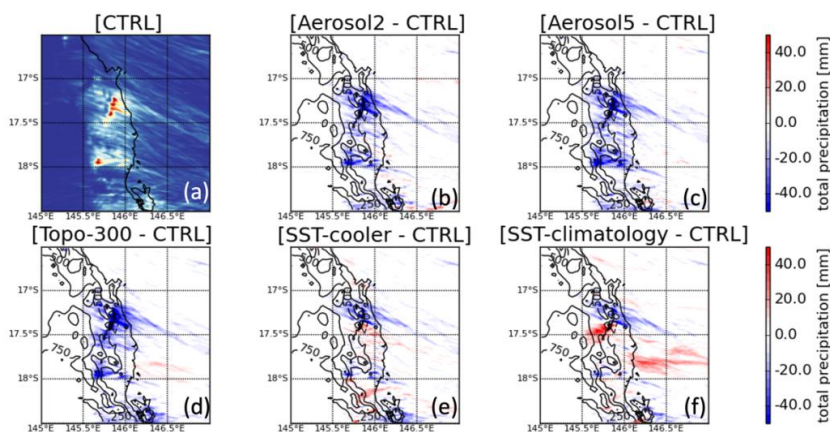
312

313 **Figure 9: (a) Accumulated precipitation for the time period of 2016-04-28 0000UTC to 2016-04-30 1200UTC from 1**

314 **km resolution with CTRL-run. (b-f) Difference plots of accumulated precipitation between CTRL-run and Aerosol2,**

315 **Aerosol-5, Topo300, SST-cooler, SST-climatology, separately. Black contours indicate the topography map from 250**

316 **to 1500 m by 250 m-interval.**

317

318 Figure 9 shows the map of accumulated precipitation over the inner-most domain from 1 km WRF simulations

319 from the CTRL-run, and the difference between CTRL-run and sensitivity studies, respectively. The accumulation

320 period is the 60-h simulation time after the spin-up (i.e. from 0000UTC 28 to 1200UTC 30 April 2016). As shown

321 in Figure 9d, a strong reduction in precipitation over the topography is evident when the topography is modified,

322 particularly over the windward slopes. Over 40 mm difference in the accumulated precipitation is noted at the

323 points of highest precipitation grids between the TOPO300 and CTRL simulations, highlighting the major role of

324 terrain in the development of precipitation. In addition to the mountain area, this precipitation reduction has also

325 been seen over the upwind region, extending to the GBR. We note a slight increase in the accumulated

326 precipitation in the southern part of the upwind domain, indicating the chaotic nature of cloud and precipitation

327 in weakly-forced locations.

328 The local cloud and precipitation differences shown in Figure 7d, 8d and 9d can be elucidated through the

329 examination of convection-related variables, including convective available potential energy (CAPE), 10 m wind

330 convergence (calculated as $(-1) \times (\partial u/\partial x + \partial v/\partial y)$, Schneider et al., 2018), and velocity difference (w_{diff}) between

331 the maximum vertical velocity below the level of free convection (LFC) and the required updraft velocity to

332 overcome convective inhibition (CIN), calculated as $\sqrt{2 \times CIN}$ (Trier 2003). Positive values of w_{diff} indicate that

333 air parcels can reach their respective LFC, release CAPE and initiate convection. Additionally, we have analysed

334 simulated trade wind inversion (TWI) properties, including its base height, thickness, and strength. This analysis

335 is important because trade-wind cumuli are constrained by the TWI, particularly over the oceanic regions. It is

336 also perhaps more difficult to directly link changes in cloud and precipitation process over the upwind domain to

337 the direct mountain-induced lifting and low-level wind convergence. Note that all these variables are calculated

338 for each grid point at each hour.

339 As seen from Figure 10a, a notable increase in CAPE is seen in the Topo300 over the downwind area, whereas

340 only small increases are found at the upwind. The change in CAPE is clearly explained by the change in orography.

341 The atmosphere deepens when the mountains are reduced, leading to higher temperatures at the surface. Because

342 the relative humidity is essentially unchanged, the LFC is lower, which results in higher CAPE values over the

343 topography in the Topo300 experiment. However, fewer grid points are simulated with positive w_{diff} in the

344 Topo300 run over the downwind area (Figure 10b), making the CAPE more challenging to release. This therefore

345 results in a reduced cloud fraction and precipitation in the Topo300, despite the presence of higher CAPE values

346 at the downwind area. Low-level wind convergence over the downwind area is much stronger in the CTRL run,

347 as the lack of strong orographic lifting in the Topo300 run produces only weak low-level convergence. However,

348 this is not as significant over the upwind area, where little to no difference in w_{diff} and low-level convergence is

349 seen between CTRL and Topo300 (Figure 10b-c).

350 As expected, the upwind area experiences weaker effects of mountain-induced lifting, and so the impacts of the

351 alteration in mountain height are attenuated. However, changes in topography do lead to modifications in the

352 upwind airstream (Chu et al., 2000; Zhang et al., 2022). Altered upwind temperature and wind profiles are likely

353 to result in modifications of TWI characteristics. It is possible that the height and thickness of trade wind inversion

354 is being modified in the Topo300, which constrains the trade cumulus development over the upwind area. To

355 explore this possibility, we compared the simulated TWI properties in the CTRL and Topo300 runs (Figure 10d-

356 f). The results show that that a higher inversion base height with a relatively larger inversion thickness is present

357 in the CTRL run over both downwind and upwind areas, whereas a reduction in orography results in a lower TWI

358 base height and a smaller inversion thickness over the upwind area. The lower TWI in the Topo300, as a result,

359 constrains the vertical development of the clouds, resulting in a lower cloud top height and less developed cloud

360 and precipitation systems. To summarize, the vertical velocity and low-level wind convergence, coupled with the

361 TWI, are crucial in explaining the cloud and precipitation features over the downwind area, which can be directly

362   linked to the mountain induced lifting and flow deviation. On the other hand, the upwind effect of orographic
363   enhancement is more closely associated with the alterations in TWI properties.
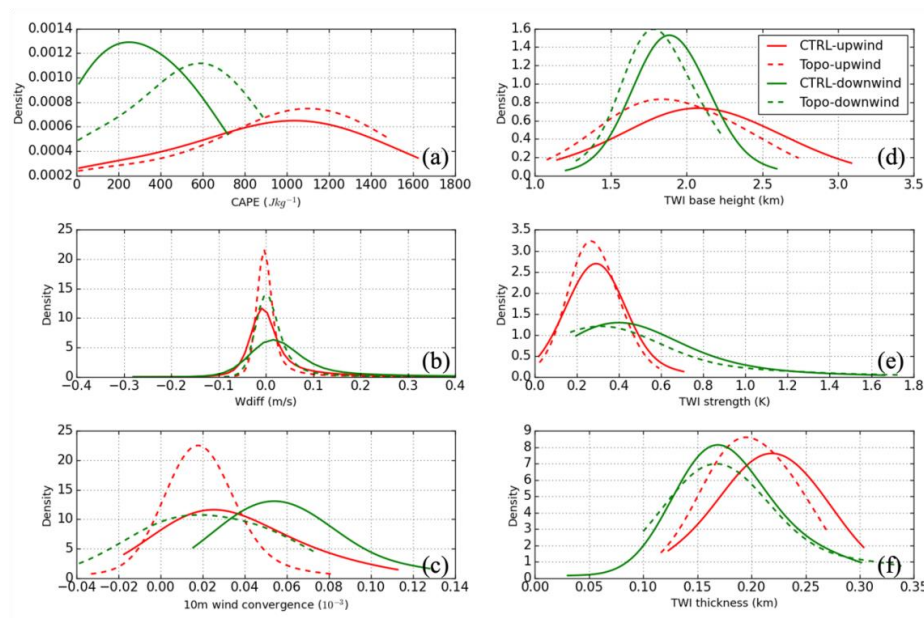
364

365   **Figure 10: PDF distribution of the (a) trade inversion base height, (b) inversion strength, (c) inversion thickness, (d)**
366   **CAPE, (e) W$_{diff}$, and (f) low-level wind convergence over the upwind (red lines) and downwind (green lines) area,**
367   **separately. The analysis covers the whole 60 h simulation period after the spin-up time. Solid lines represent results**
368   **from CTRL, and dashed lines are for Topo300 sensitivity experiment.**

369

5.2 Local aerosol loading

371   We have also explored the hypothesis that regional aerosol loading may affect the cloud and precipitation
372   properties over the GBR. As shown in Figure 11a, doubling the surface WFA emission over the GBR (Aerosol2
373   experiment) results in an increase of ~700/cm^3 in the near-surface WFA number concentration over the upwind
374   sub-domain (from 572/cm^3 to 1250/cm^3), throughout the evolution of the simulation. The increase in WFA
375   emission at the surface also leads to an increase in the atmospheric WFA population to levels above 2 km (Figure
376   13a). Pertaining to the Aerosol5 experiment, the near-surface WFA number concentration increases by
377   approximately 1400/cm^3, from 572/cm^3 to 2241/cm^3, in comparison to the CTRL (Figure 11a) as well as an
378   enhancement in the upper-level profile of the WFA concentration (Figure 13e). A slight time-variation in WFA
379   number concentration (WFANC) is seen for both Aerosol2 and Aerosol5, which primarily results from the
380   advection and diffusion of the aerosol during the model integration (Thompson and Eidhammer, 2014). The
381   notable spike of the WFA number concentration during the last day of the simulation is primarily attributed to the
382   strong inflow from the southern portion of the GBR when the surface wind changes from easterly to southeasterly
383   (Figure 4). It is worth noting that a fairly similar increase in the WFANC is also seen over the downwind

384   subdomain in both Aerosol sensitivity experiments (Figure 12a, Figure 13a and 13e). Given the predominance of

385   trade wind patterns in this region, this downwind impact is not unexpected.

386   Cloud droplet number concentration (CDNC), considered both upwind and downwind, is sensitive to the changes

387   in the atmospheric aerosol number concentration (Figure 11b and 12b). A higher CDNC corresponds to an increase

388   in the WFA population is evident from the cloud base to the cloud top (Figure 13b and 13f). Total CF, however,

389   is found to be essentially unaffected by the changes in the aerosol concentration over both sub-domains (Figure

390   11c and 12c). The vertical profile of CF over the upwind subdomain (Figure 13c) suggests a slight deepening of

391   the trade cumulus with an increase in domain-averaged CF at cloud top, especially in Aerosol5 experiment (also

392   shown in Figure 8c). Minimal response is seen at cloud base. This is consistent with an increase of the liquid water

393   path (LWP), which is evident in both the Aerosol2 and Aerosol5 experiments (Figure 11d and 13d) over the

394   upwind. Looking downwind, even though the CF remains largely unchanged across the altitudes (Figure 13g, 7b

395   and 7c), a cloudy layer with higher CDNC could also result in a larger LWP as shown in Figure 12d. Additionally,

396   the cloud radiative effect (CRE) has been considered through the CTRL run and the Aerosol sensitivity

397   experiments. CRE is defined as the net radiation flux (downward flux minus upward flux) under all sky conditions

398   minus the net radiation flux under clear sky conditions and can be applied to both the surface and top of atmosphere

399   (Imre et al., 1996; Bao et al., 2020). Here, in this analysis, we focus on the shortwave CRE (SWCRE) at the

400   surface, as it represents the effective solar heating of the sea surface. As shown in Figure 11e and 12e, a rise in

401   SWCRE, though small with a maximum of 50 W/m^2, is evident with increase in aerosol population over both sub-

402   domains. This is primarily attributed to the higher CDNC, as the cloud reflectance is enhanced with increased

403   droplets number concentration.

404   As shown in Figure 9b and 9c, a reduction in total precipitation is seen in both Aerosol sensitivity experiments,

405   primarily over the downwind mountain area, with a maximum 30mm difference (~30% reduction) noted around

406   the peak precipitation points. This decreased precipitation is evident throughout the simulation hours between the

407   CTRL and Aerosol sensitivity runs (Figure 12f). Relatively small changes (less than 20 mm) in accumulated

408   precipitation are seen over the upwind area, where the decreased accumulated precipitation mainly originates from

409   a few hours in the last day of simulation (Figure 11f). Although small in magnitude, the warm cloud precipitation

410   over the GBR is found to show considerable responses to the changes in the local aerosol loading.

411   Increased CCN concentrations can be expected to produce smaller droplets for a given liquid water content

412   (Twomey, 1997). The smaller cloud droplets can reduce the efficiency of collision and coalescence, which may

413   inhibit precipitation development (Albrecht, 1989). Over the GBR, our sensitivity experiment indicates

414   consistently that, cloud microphysical properties, including CDNC and LWP, and precipitation respond strongly

415   to changes in the local WFANC. A significant rise in CDNC is correlated with an increase in the aerosol

416   population is seen over the GBR, and predominantly leads to suppressed precipitation over both upwind and

417   downwind areas. While the total CF is showing less sensitivity to the aerosol perturbations. It's worth noting that

418   the Aerosol sensitivity experiments also show evidence of deepened trade cumulus over the upwind region, which

419   will increase the LWP and the SWCRE. A notable downwind effect featured by a significant reduction of surface

420   precipitation is simulated when changing the surface aerosol emissions over the GBR.

421 We note that how convection may interact with changes in aerosol is still a large source of uncertainty (Tao et al.,

422 2012) and our experiment only focus on perturbing the water friendly aerosol loading over the GBR. Previous

423 studies have shown that the thermodynamic environment is strongly modulated by the large-scale forcing, whose

424 impact on the cloud field might surpass that of local aerosol perturbations (Dagan et al., 2018; Spill et al., 2021).

425 Spill et al. (2021) show that the response of cumulus cloud and precipitation to the aerosol perturbation is much

426 stronger in the idealised simulations without the large-scale forcing. This suggests a potentially limited effect of

427 aerosols on cumulus cloud fields in the realistic condition due to the predominant influence of large-scale forcing.

428 The nature variability of the marine shallow clouds and precipitation process could also explain some of the

429 differences between the CTRL and Aerosol sensitivity runs.
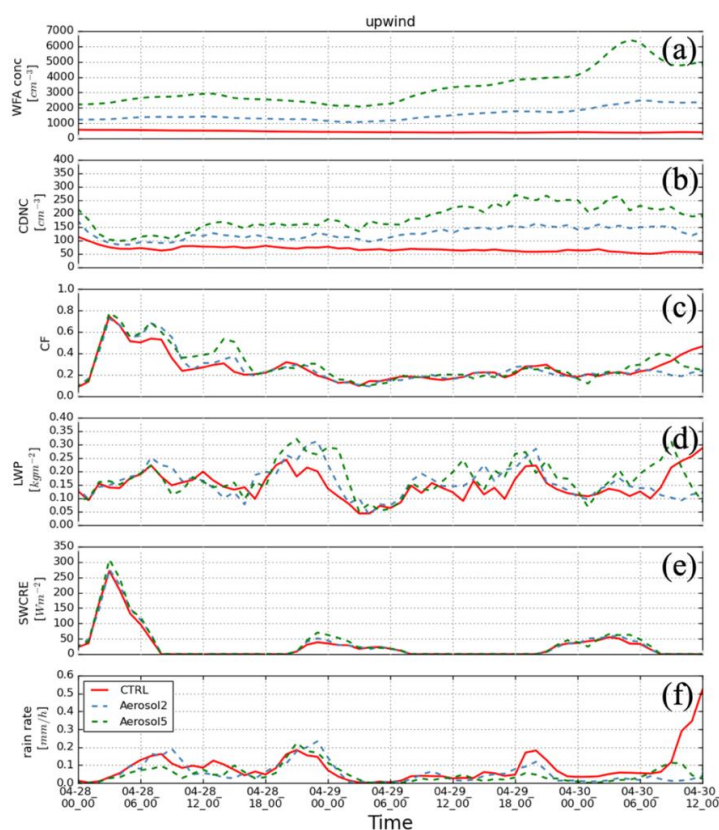
430

431 **Figure 11: Time series of domain-averaged (a) water-friendly aerosol number concentration, (b) cloud droplet number**

432 **concentration, (c) cloud fraction, (d) liquid water path, (e) shortwave cloud radiative effect, and (f) rain rate from 1 km**

433 **resolution with CTRL (red solid lines), Aerosol2 (blue dashed lines), and Aerosol5 (green dashed lines). The target area**

434 **is over upwind sub-domain.**
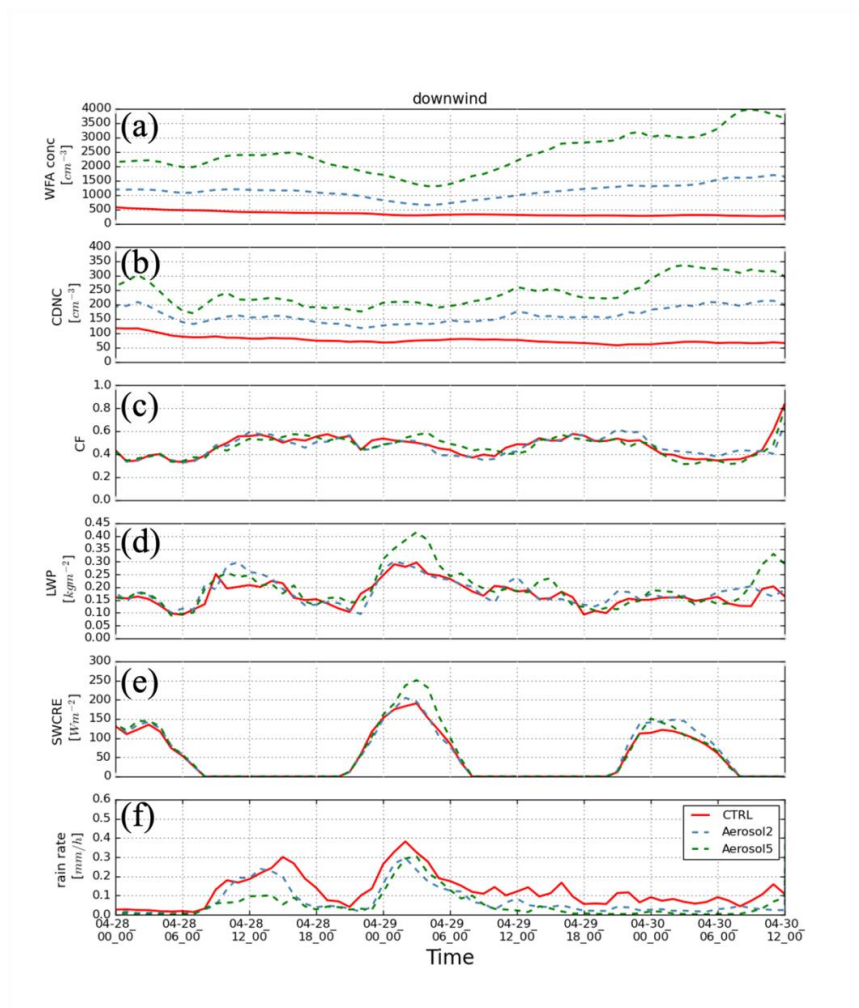
435

436 **Figure 12: Same as Figure 11, but for downwind sub-domain.**
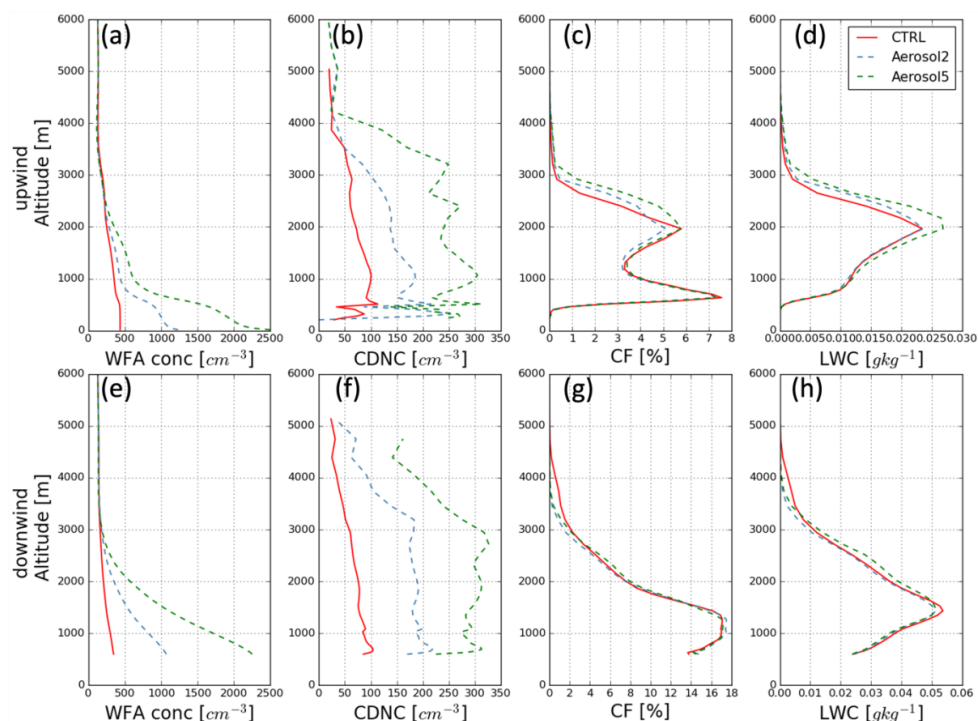
Figure 13: Vertical profiles of (a) domain-averaged water-friendly aerosol number concentration, (b) in-cloud averaged cloud droplet number concentration, (c) domain-averaged cloud fraction, and (d) domain-averaged liquid water content over the upwind sub-domain from CTRL (in red), Aerosol2 (in blue), and Aerosol5 (in green). The analysis is for 60h simulation time after the spin-up from 2016-04-28 0000UTC to 2016-04-30 1200UTC. (e-h) same as (a-d), but for downwind sub-domain.

5.3 Local SST forcing

In this section, we have explored the sensitivity of cloud and precipitation properties over the GBR in response to the local SST changes. It is important to note that, unlike the SST alteration in the SST-cooler experiment, part of the ocean area in the SST-climatology is warmer than the actual SST at the beginning of the simulation (Figure S2). Nevertheless, the sea surface temperature over the majority of the GBR is reduced in the SST-climatology experiment.

A reduction in CF is noted over the upwind in the SST-cooler run, with the most notable difference apparent at lower altitudes (Figure 8e). This small decrease in CF might be associated with a consistent decrease in surface heat flux and moisture flux in the SST-cooler experiment (Figure 14). Over the downwind sub-domain, the CF has only a small difference between the CTRL and SST-cooler experiments (Figure 7e). However, a decrease in the accumulated precipitation is discernible over downwind points with the peak accumulated precipitation (Figure 9e). Similar but more variable findings are evident from the SST-climatology experiment. Figure 7f shows small but more complex changes in CF in the downwind area with associated positive and negative changes in

457 accumulated precipitation (Figure 9f). These variable impacts are likely due to the non-uniform (positive and

458 negative) changes in SST associated with the differences between the CTRL and SST-climatology runs. (Figure

459 S2). The downwind effect on precipitation is similarly discernible in the SST-climatology, however there are no

460 noteworthy results related to the cloud fraction (Figure 7f). There is a minor decrease in averaged surface heat

461 flux and moisture flux in the SST-climatology experiment (Figure 14). However, a notable number of grid points

462 have larger values, potentially associated with the warmer water over the southern part of ocean domain in the

463 SST-climatology run (Figure S1).

464 Theoretically, a warmer SST will likely provide more water vapor in the atmosphere through increased surface

465 latent heat fluxes. The increased atmospheric water vapor, under such conditions, will consequently induce more

466 rainfall at local and downstream regions. Over the tropics, the SST has been noted in several studies to be a key

467 factor controlling the location of rainfall over various timescales (Lu and Lu, 2014; Jo et al., 2019; Wu et al., 2009;

468 Wu and Kirtman, 2007). Takahashi and Dado (2018) highlight the impact of local and/or nearby SST on local and

469 regional climate. In particular, they found that warmer local SST results in greater rainfall over the downstream

470 land region in the mid-latitudes based on observational dataset, which suggests strong air-sea coupling processes.

471 Our numerical sensitivity experiments, to some extent, show consistent results, indicating that precipitation over

472 the GBR shows response to the underlying SST conditions, though the effect is weak on the scales considered

473 here. A downwind effect on the precipitation has been found over the Wet Tropics. Sensitivity of cloud fraction

474 in response to SST variation is seen over the water area, though the magnitude is minor in comparison with the

475 major orographic impacts. The relationship between cloud fraction and SST in the lower levels have been found

476 to largely depend on the type of cloud and its height (Cesana et al., 2019). Stronger response of "lower-top"

477 shallow cloud properties (i.e. stratocumulus) to the changes in SST is noted in Cesana et al. (2019) in comparison

478 with "higher-top" shallow clouds, for example, cumulus. As such, much minor responses to the changes in SST

479 are expected when considering cloud fields with the higher cloud tops. In our experiment, instances of simulated

480 cloud field with cloud tops over 3km could largely contribute to the variety of the responses to SST forcing.

481 Overall, our simulations suggest that warm-cloud precipitation over the GBR is sensitive to the underlying local

482 SST forcing, though the responses are weak on the scales considered in this study. Our work supports the

483 important role of local SST on the regional climate over the GBR, but further work on understanding the synoptic

484 and thermodynamic background and air-sea coupling processes is necessary to help elucidate the mechanisms

485 involved.

486

487
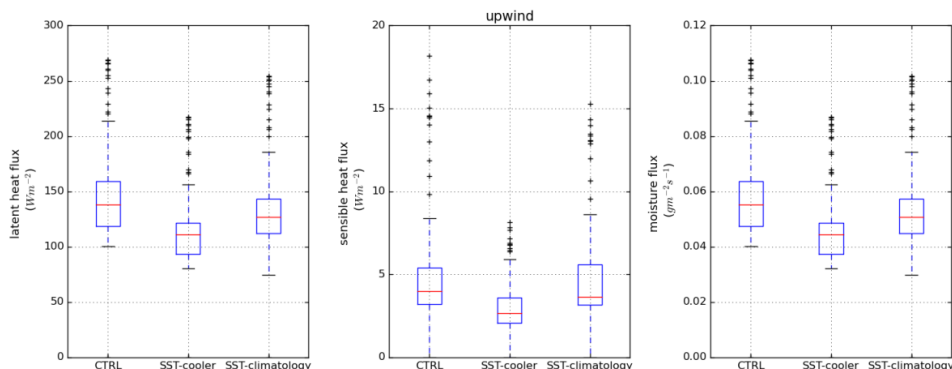
Figure 14: Boxplots showing the comparison of latent heat flux, sensible heat flux, and moisture flux from 1 km resolution simulation with CTRL, SST-cooler, and SST-climatology. The analysis is for 60h simulation period, and over the upwind sub-domain.

491

6 Summary and conclusions

A primary aim of this research is to study the sensitivity of trade cumulus precipitation to different local forcings over the GBR using a case study of an orographic precipitation event associated with low-level trade cumulus at the end of April 2016. The selected days for the simulations are characterised by well-defined cumulus and stratocumulus under the trade wind regime without any overlying high clouds. These trade cumuli are observed to generate precipitation over the Wet Tropics around Townsville.

The large-scale meteorology is well captured in the CTRL simulation in terms of the location, duration and magnitude of the surface pressure system and wind fields. Comparison of the upper air profiles from both Townsville and Wills Island sounding stations showed good agreement in wind speed, wind direction and temperature profiles. The CTRL simulation also demonstrated a considerable level of skill in simulating both the spatial distribution and the intensity of precipitation over the Wet Tropics as compared to ground observations.

Sensitivity experiments are conducted to investigate the sensitivity of trade cumulus and precipitation in response to the local forcings. Our major findings from the sensitivity analysis are summarized as follows:

- Reducing the elevation above 300m by 75% decreases the cloud fraction and accumulated precipitation over the Wet Tropics, including both downwind and upwind areas. Weaker vertical velocity and low-level wind convergence are generated in the Topo300 run over the downwind sub-domain, suggesting their crucial role in rainfall production. The reduced TWI base height in the Topo300 run is found to limit the cloud-precipitation development over the upwind water area.

- Cloud microphysical properties, including CDNC, LWP, and precipitation are sensitive to the changes in atmospheric aerosol population over the GBR. Higher CDNC and LWP correlated to increased aerosol number concentration leads to a rise in SWCRE, though the magnitude is small, over both sub-domains.

513   Although CF remains largely unchanged, a deepened cloud is evident over the upwind when WFANC is
514   increased. A downwind effect on cloud and precipitation properties is further noted.
515 • Cloud fraction and total precipitation over the GBR show a small response to the underlying local SST
516   forcing. A reduction in cloud fraction is noted over the upwind water area when the initial SST is reduced,
517   but any difference is negligible over the downstream orographic region. There is a decrease in the
518   accumulated precipitation in the SST sensitivity experiments over downwind girds where the peak
519   accumulated precipitation generated. These small decreases in cloud fraction and accumulated
520   precipitation are likely associated with the consistently decreased surface heat flux and moisture flux in
521   the SST experiments.

522 Although a range of responses of cloud and precipitation to the local forcings are produced across the GBR in our
523 simulations, it is recognised that ensemble analysis is necessary in the future to better represent the natural
524 variability of these trade clouds and precipitation properties. In situ observations will also be necessary to help
525 investigate the detailed lifecycle of these low-level clouds and the development of the topographic precipitation.
526 Furthermore, there is a need to carry out case studies during the time of intense SST increases that may induce
527 thermal coral bleaching over the GBR. Nevertheless, our analysis sheds some light on understanding the
528 interactions between trade wind cumuli and local forcings across the GBR and Wet Tropics, where the importance
529 of the local low-level cloud in thermal coral bleaching has recently been identified.

Data availability statement

All data sets used in this study are freely and publicly available online and may be accessed directly as follows. The University of Wyoming upper-air sounding is downloaded from http://weather.uwyo.edu/upperair/sounding.html. The ERA5 reanalysis data is available at the website: https://cds.climate.copernicus.eu/cdsapp#!/search?-type=dataset. The Australian Bureau of Meteorology Daily rainfall can be downloaded from the website: http://www.bom.gov.au/climate/data/index.shtml. The Himawari-8 full disk observational products are available at NCI THREDDS Data Server: https://dapds00.nci.org.au/thredds/catalogs/ra22/satellite-products/arc/obs/himawari-ahi/fldk/fldk.html. The Himawari-8 true color imagery and cloud types classification are available at JAXA Himawari Monitor supplied by P-Tree System: https://www.eorc.jaxa.jp/ptree/.

Author contribution: W.Z., Y.H., S.S. and M.M. developed the ideas and designed the study. W.Z. collected the data, performed the analysis and prepared the draft manuscript. Y.H., S.S., M.M. and D.H. supervised and reviewed the manuscript. All authors made substantial contributions to this work and approved the final version of the manuscript.

Competing Interests: Some authors are members of the editorial board of journal Atmospheric Chemistry and Physics.

Acknowledgments: This work is supported by Reef Restoration and Adaptation Program which is founded by the partnership between the Australian Governments Reef Trust and the Great Barrier Reef Foundation. Wenhui Zhao was also supported by Monash Graduate scholarship while working at Monash University. Yi Huang, and Steve Siems are further supported by Australian Research Council Discovery Grant (ARC DP230100639). The Australian National Computational Infrastructure is also thanked for providing the computational resources. We have also benefited from discussions with Greg Thompson. The authors would like to acknowledge the Traditional Owners of the Great Barrier Reef, particularly the Wulgurukaba and Bindal people of the Townsville region nearby the area of our case study.

555   **References**
556

557   Albrecht, B. A.: A model study of downstream variations of the thermodynamic structure of the trade winds.
558   Tellus A, 36 (2), 187–202, 1984.

559   Albrecht, B. A.: Aerosols, cloud microphysics, and fractional cloudiness. Science, 245(4923), 1227–1230.
560   https://doi.org/10.1126/ science.245.4923.1227, 1989.

561   Bao, Shanhu, Letu, Husi, Zhao, Jun, Lei, Yonghui, Zhao, Chuanfeng, Li, Jiming, Tana, Gegen, Liu, Chao, Guo,
562   Enliang, Zhang, Jie, He, Jie, and Bao, Yuhai: Spatiotemporal distributions of cloud radiative forcing and
563   response to cloud parameters over the Mongolian Plateau during 2003–2017. International Journal of
564   Climatology, 40(9), 4082–4101. https://doi.org/10.1002/joc.6444, 2020.

565   Berkelmans, R., G. De'ath, S. Kininmonth, and W. J. Skirving: A comparison of the 1998 and 2002 coral
566   bleaching events on the Great Barrier Reef: Spatial correlation, patterns and predictions, Coral Reefs, 23,
567   74 – 83. https://doi.org/10.1007/s00338-003- 0353-y, 2004.

568   Bonell, M. and D. Gilmour: Variations in short-term rainfall intensity in relation to synoptic climatological aspect
569   of the humid tropical northeast Queensland coast. Singapore Journal of Tropical Geography, 1 (2), 16–
570   30, 1980.

571   Bony, S., Dufresne, J.-L., Le Treut, H., Morcrette, J.-J. and Senior, C.: On dynamic and thermodynamic
572   components of cloud changes. Climate Dynamics, 22(2–3), 71–86. https:// doi.org/10.1007/s00382-003-
573   0369-6, 2004.

574   Boucher, O., D. Randall, P. Artaxo, C. Bretherton, G. Feingold, P. Forster, V.-M. Kerminen, Y. Kondo, H. Liao,
575   U. Lohmann, P. Rasch, S.K. Satheesh, S. Sherwood, B. Stevens and X.Y. Zhang: Clouds and Aerosols.
576   In: Climate Change 2013: The Physical Science Basis. Contribution of Working Group I to the Fifth
577   Assessment Report of the Intergovernmental Panel on Climate Change (IPCC), Cambridge University
578   Press, Cambridge, vol 5, pp 571–657, 2013.

579   Bureau of Meteorology: Himawari 8/9 Full Disk Observations – Archive (ARC) data stream. NCI Australia.
580   (Dataset) https://dx.doi.org/10.25914/61a609aa1434d, 2021.

581   Colarco, P., A. da Silva, M. Chin, and T. Diehl: Online simulations of global aerosol distributions in the NASA
582   GEOS-4 model and comparisons to satellite and ground-based aerosol optical depth. J. Geophys. Res.,
583   115, D14207, doi:10.1029/2009JD012820, 2010.

584   Cesana, G., Del Genio, A.D., Ackerman, A.S., Kelley, M., Elsaesser, G., Fridlind, A.M., Cheng, Y. and Yao,
585   M.S.: Evaluating models' response of tropical low clouds to SST forcings using CALIPSO observations.
586   Atmospheric Chemistry and Physics, 19(5), pp.2813-2832, https://doi.org/10.5194/acp-19-2813-2019,
587   2019.

588   Chen, F., and J. Dudhia: Coupling an advanced landsurface/hydrology model with the Penn State/NCAR MM5
589   modeling system. Part I: Model description and implementation. Mon. Wea. Rev., 129, 569–585, doi:
590   10.1175/1520- 0493(2001)1292.0.CO;2, 2001.

591   Chen, T., W. B. Rossow, and Y. C. Zhang: Radiative effects of cloud-type variations, J. Clim., 13, 264-286,
592   https://doi.org/10.1175/1520-0442(2000)013<0264:REOCTV>2.0.CO;2, 2000.

593   Chu, C. M., and Lin, Y. L.: Effects of orography on the generation and propagation of mesoscale convective
594   systems in a two-dimensional conditionally unstable flow. Journal of the atmospheric sciences, 57(23),
595   3817-3837, https://doi.org/10.1175/1520-0469(2001)057<3817:EOOOTG>2.0.CO;2, 2000.

596   Colarco, P., A. da Silva, M. Chin, and T. Diehl: Online simulations of global aerosol distributions in the NASA
597   GEOS-4 model and comparisons to satellite and ground-based aerosol optical depth. J. Geophys. Res.,
598   115, D14207, doi:10.1029/2009JD012820, 2010.

599   Colle, B.A., Wolfe, J.B., Steenburgh, W.J., Kingsmill, D.E., Cox, J.A.W., and Shafer, J.C.: High-resolution
600   simulations and microphysical validation of an orographic precipitation Event over the Wasatch
601   Mountains   during   IPEX   IOP3.   Mon.   Weather   Rev.   133,   2947–2971.
602   https://doi.org/10.1175/MWR3017.1, 2005.

Crook, N. A.: Sensitivity of moist convection forced by boundary layer processes to low-level thermodynamic fields. Monthly Weather Review, 124(8), 1767-1785, 1996.

Cropp, Roger, Gabric, Albert, van Tran, Dien, Jones, Graham, Swan, Hilton, and Butler, Harry: Coral reef aerosol emissions in response to irradiance stress in the Great Barrier Reef, Australia. Ambio, 47(6), 671–681. https://doi.org/10.1007/s13280-018-1018-y, 2018.

Dagan, G., Koren, I., Altaratz, O., and Lehahn, Y.: Shallow convective cloud field lifetime as a key factor for evaluating aerosol effects. iScience, 10, 192–202. https://doi.org/10.1016/j.isci.2018.11.032, 2018.

Deschaseaux, E., E. Deschaseaux, G. Jones, and H. Swan: Dimethylated sulfur compounds in coral-reef ecosystems. Environmental Chemistry 13: 239–251. https://doi.org/10.1071/ en14258, 2016.

Eastman, R., Warren, S. G., and Hahn, C. J.: Variations in cloud cover and cloud types over the ocean from surface observations. 1954–2008, Journal of Climate, 24, 5914– 5934. https://doi.org/10.1175/2011JCLI3972.1, 2011.

Eleftheratos, K., Zerefos, C. S., Varotsos, C., and Kapsomenakis, I.: Interannual variability of cirrus clouds in the tropics in El Niño Southern Oscillation (ENSO) regions based on International Satellite Cloud Climatology Project (ISCCP) satellite data. International Journal of Remote Sensing, 32(21), 6395–6405. https://doi.org/10.1080/01431161.2010.510491, 2011.

Fiddes, Sonya L, Woodhouse, Matthew T, Lane, Todd P, and Schofield, Robyn: Coral- reef-derived dimethyl sulfide and the climatic impact of the loss of coral reefs. Atmospheric Chemistry and Physics, 21(8), 5883–5903. https://doi.org/10.5194/acp-21-5883-2021, 2021.

Filipiak, M. J., Merchant, C. J., Kettle, H., and Le Borgne, P.: An empirical model for the statistics of sea surface diurnal warming. Ocean Science, 8(2), 197-209, https://doi.org/10.5194/os-8-197-2012, 2012.

Fischer E, and Jones G.: Atmospheric dimethysulphide production from corals in the Great Barrier Reef and links to solar radiation, climate and coral bleaching. Biogeochemistry 110: 31–46, 2012.

Gentemann, C. L., C. J. Donlon, A. Stuart-Menteth, and F. J. Wentz: Diurnal signals in satellite sea surface temperature measurements, Geophys. Res. Lett., 30(3), 1140, doi:10.1029/2002GL016291, 2003.

Herwitz, S.R.: Infiltration-excess caused by Stemflow in a cyclone-prone tropical rainforest. Earth Surface Processes and Landforms, 11(4), 401–412. https://doi.org/10.1002/esp. 3290110406, 1986.

Hersbach, H., de Rosnay, P., Bell, B., Schepers, D., Simmons, A., Soci, C., Abdalla, S., Alonso-Balmaseda, M., Balsamo, G., Bechtold, P. and Berrisfold, P.: Operational global reanalysis: Progress, future directions and synergies with NWP. ECMWF ERA Report Series, 27, 65, doi: 10.21957/tkic6g3wm, 2018.

Hersbach, H., Bell, B., Berrisford, P., Hirahara, S., Horányi, A., Muñoz-Sabater, J., Nicolas, J., Peubey, C., Radu, R., Schepers, D. and Simmons, A.: The ERA5 global reanalysis. Quarterly Journal of the Royal Meteorological Society, 146(730), 1999-2049, https://doi.org/10.1002/qj.3803, 2020.

Hughes, T.P., Kerry, J.T., Álvarez-Noriega, M., Álvarez-Romero, J.G., Anderson, K.D., Baird, A.H., Babcock, R.C., Beger, M., Bellwood, D.R., Berkelmans, R. and Bridge, T.C.: Global warming and recurrent mass bleaching of corals. Nature, 543(7645), 373–377. https://doi.org/10.1038/nature21707, 2017.

Hong, Song-You, Yign Noh, and Jimy Dudhia: A new vertical diffusion package with an explicit treatment of entrainment processes. Monthly weather review 134.9, 2318- 2341, https://doi.org/10.1175/MWR3199.1, 2006.

Houze, R.A.: Orographic effects on precipitating clouds. Rev. Geophys. 50 RG1001, 47pp, https:// doi.org/10.1029/2011RG000365, 2012.

Imre, D., Abramson, E. and Daum, P.: Quantifying Cloud Induced Shortwave Absorption: An Examination of Uncertainties and of Recent Arguments for Large Excess Absorption. Journal of Applied Meteorology (1988–2005), 35(11), 1991–2010. https://doi.org/10.1175/1520-0450(1996)0352. 0.CO;2, 1996.

Janjić, Zaviša I.: Comments on "Development and evaluation of a convection scheme for use in climate models". Journal of the Atmospheric Sciences 57.21:3686-3686, https://doi.org/10.1175/1520-0469(2000)057<3686:CODAEO>2.0.CO;2 , 2000.

Jo, H. S., Yeh, S. W., and Cai, W.: An episodic weakening in the boreal spring SST– precipitation relationship in the western tropical Pacific since the late 1990s. Journal of Climate, 32(13), 3837-3845, https://doi.org/10.1175/JCLI-D-17-0737.1, 2019.

Jones, G., Curran, M., Swan, H. and Deschaseaux, E.: Dimethylsulfide and Coral Bleaching: Links to Solar Radiation, Low Level Cloud and the Regulation of Seawater Temperatures and Climate in the Great Barrier Reef. American Journal of Climate Change, 6, 328-359. doi: 10.4236/ajcc.2017.62017, 2017.

Jones, G.B.: The reef sulphur cycle: Influence on climate and ecosystem services. In Ethnobiology of corals and coral reefs, ed. N.E. Narchi, and L.L. Price, 27–57. Cham: Springer, doi: 10.1007/978-3-319-23763-3_3, 2015.

Leahy, S. M., Kingsford, M. J., and Steinberg, C. R.: Do clouds save the Great Barrier Reef? Satellite imagery elucidates the cloud-SST relationship at the local scale. PLoS One, 8(7), e70400, https://doi.org/10.1371/journal.pone.0070400, 2013.

Lohmann, U, and Feichter, J.: Global indirect aerosol effects: A review. Atmospheric Chemistry and Physics, 5(3), 715–737. https://doi.org/10.5194/acp-5-715-2005, 2005.

Lu, R., and S. Lu: Local and remote factors affecting the SST– precipitation relationship over the western North Pacific during summer. J. Climate, 27, 5132–5147, https://doi.org/ 10.1175/JCLI-D-13-00510.1, 2014.

Mumby, P., Chisholm, J., Edwards, A., Andrefouet, S., and Jaubert, J.: Cloudy weather may have saved Society Island reef corals during the 1998 ENSO event, Marine Ecology Progress Series, 222, 209–216, https://doi.org/10.3354/meps222209, 2001.

Murphy, M J.: Variability in the trade wind regime and wet season of Northeastern Queensland, 2017.

Mlawer, E. J., Taubman, S. J., Brown, P. D., Iacono, M. J., and Clough, S. A.: Radiative transfer for inhomogeneous atmospheres: RRTM, a validated correlated-k model for the longwave. J. Geophys. Res. Atmos., 102, 16663, doi: 10.1029/97JD00237, 1997.

M. J. Weston, S. J. Piketh, F. Burnet, S. Broccardo, C. Denjean, T. Bourrianne, and P. Formenti: Sensitivity analysis of an aerosol-aware microphysics scheme in Weather Research and Forecasting (WRF) during case studies of fog in Namibia. Atmospheric Chemistry and Physics, 22, 10221–10245. https://doi.org/10.5194/acp-22-10221-2022, 2022.

Norris, J. R.: Low cloud type over the ocean from surface observations. Part II: Geographical and seasonal variations. Journal of climate, 11(3), 383-403, https://doi.org/10.1175/1520-0442(1998)011<0383:LCTOTO>2.0.CO;2, 1998.

Qu X, Hall A, Klein SA, and DeAngelis AM: Positive tropical marine low-cloud cover feedback inferred from cloud-controlling factors. Geophys Res Lett 42:7767–7775. Https://doi. org/10.1002/2015GL065627, 2015.

Rauber, R. M., Stevens, B., Ochs, H. T., Knight, C. A., Albrecht, B. A., Blyth, A. M., Fairall, C. W., and Jensen, J. B., Lasher-Trapp, S.G., Mayol-Bracero, O.L. and Vali, G.: Rain in shallow cumulus over the ocean: The RICO campaign. Bulletin of the American Meteorological Society, December 2007, 1912–1928. https://doi.org/10.1175/BAMS-88-12-1912, 2007.

Riehl, Herbert. Climate and Weather in the Tropics. Academic Press, 1979.

Roe, G.H.: Orographic precipitation. Annu. Rev. Earth Planet. Sci. 33, 645–671. https://doi.org/10.1146/annurev.earth.33.092203.122541, 2005.

Sarmadi, F., Huang, Y., Thompson, G., Siems, S. T., and Manton, M. J.: Simulations of orographic precipitation in the Snowy Mountains of Southeastern Australia. Atmospheric Research, 219, 183-199, https://doi.org/10.1016/j.atmosres.2019.01.002, 2019.

Schneider, L., Barthlott, C., Barrett, A. I., and Hoose, C.: The precipitation response to variable terrain forcing over low mountain ranges in different weather regimes. Quarterly Journal of the Royal Meteorological Society, 144(713), 970-989, https://doi.org/10.1002/qj.3250, 2018.

Skamarock, W.C., Klemp, J.B., Dudhia, J., Gill, D.O., Liu, Z., Berner, J., Wang, W., Powers, J.G., Duda, M.G., Barker, D.M. and Huang, X.Y.: A description of the advanced research WRF version 4. NCAR tech. note ncar/tn-556+ str, 145, 2019.

Spill, G., Stier, P., Field, P. R., and Dagan, G.: Contrasting responses of idealised and realistic simulations of shallow cumuli to aerosol perturbations. Geophysical Research Letters, 48, e2021GL094137. https://doi.org/10.1029/2021GL094137, 2021.

Stevens B and Brenguier J-L: Cloud-controlling factors: low clouds Clouds in the Perturbed Climate System: Their Relationship to Energy Balance, Atmospheric Dynamics, and Precipitation ed J Heintzenberg and R J Charlson (Cambridge, MA: MIT Press) pp 173–196, https://doi.org/10.7551/mitpress/9780262012874.003.0008, 2009.

Stuart-Smith, R. D., Brown, C. J., Ceccarelli, D. M., and Edgar, G. J.: Ecosystem restructuring along the Great Barrier Reef following mass coral bleaching. Nature (London), 560(7716), 92–96. https://doi.org/10.1038/s41586-018-0359-9, 2018.

Sumner, G. and M. Bonell: Circulation and daily rainfall in the North Queensland wet seasons 1979–1982. Journal of Climatology, 6 (5), 531–549, https://doi.org/10.1002/joc.3370060507, 1986.

Smith, S.A., Vosper, S.B., and Field, P.R.: Sensitivity of orographic precipitation enhancement to horizontal resolution in the operational Met Office Weather forecasts. Meteorol. Appl. 22, 14–24. https://doi.org/10.1002/met.1352, 2015.

Takahashi, Naoya, Hayasaka, Tadahiro, Qiu, Bo, and Yamaguchi, Ryohei: Observed response of marine boundary layer cloud to the interannual variations of summertime Oyashio extension SST front. Climate Dynamics, 56(11-12), 3511–3526. https://doi.org/10.1007/s00382-021-05649-4, 2021.

Tao, W. K., Chen, J.-P., Li, Z., Wang, C., and Zhang, C.: Impact of Aerosols on boundary layer clouds and precipitation, Reviews of Geophysics, 50, 2011RG000 369, https://doi.org/10.1029/2011RG000369.1.INTRODUCTION, 2012.

Thompson, G., and Eidhammer, T.: A study of aerosol impacts on clouds and precipitation development in a large winter cyclone. Journal of the atmospheric sciences, 71(10), 3636-3658, https://doi.org/10.1175/JAS-D-13-0305.1, 2014.

Tian, Baijun, Waliser, Duane E, and Fetzer, Eric J.: Modulation of the diurnal cycle of tropical deep convective clouds by the MJO. Geophysical Research Letters, 33(20). https://doi.org/10.1029/2006GL027752, 2006.

Trier, S.B.: Convective storms – convective initiation. In: Holton, J.R., Curry, J.A. and Pyle, J.A. (Eds.) Encyclopedia of Atmospheric Sciences, Vol. 2. London: Academic Press, pp. 560–570, 2003.

Twomey, S.: The influence of pollution on the shortwave albedo of clouds. Journal of the Atmospheric Sciences, 34(7), 1149–1152. https://doi.org/10.1175/1520-0469(1977)034<1149:TIOPOT>2.0.CO;2, 1977.

Warren, S G, Hahn, C J, London, J, Chervin, R M, and Jenne, R L.: Colorado Univ., Boulder, CO, Colorado Univ., Boulder, CO, and National Center for Atmospheric Research, Boulder, CO. Global distribution of total cloud cover and cloud type amounts over the ocean. United States: N. p., Web. doi:10.2172/5415329, 1988.

Weston, M., Piketh, S., Burnet, F., Broccardo, S., Formenti, P., and Laplace, S.: Sensitivity analysis of an aerosol aware microphysics scheme in WRF during case studies of fog in Namibia. Mesoscale model parameterisation of fog in arid environments, 129, https://doi.org/10.5194/acp-22-10221-2022, 2022.

Wheeler, M. C., and Hendon, H. H.: An all-season real-time multivariate MJO index: Development of an index for monitoring and prediction. Monthly weather review, 132(8), 1917-1932, https://doi.org/10.1175/1520-0493(2004)132<1917:AARMMI>2.0.CO;2, 2004.

Wilkinson, J. M., Porson, A. N. F., Bornemann, F. J., Weeks, M., Field, P. R., and Lock, A. P.: Improved microphysical parametrization of drizzle and fog for operational forecasting using the Met Office Unified Model, Q. J. Roy. Meteorol. Soc., 139, 488–500, https://doi.org/10.1002/qj.1975, 2013.

Wu, B., T. Zhou, and T. Li: Contrast of rainfall–SST relationships in the western North Pacific between the ENSO-developing and ENSO-decaying summers. J. Climate, 22, 4398–4405, https://doi.org/10.1175/2009JCLI2648.1, 2009.

Wu, R., and B. P. Kirtman: Regimes of seasonal air–sea interaction and implications for performance of forced simulations. Climate Dyn., 29, 393–410, https://doi.org/10.1007/s00382-007-0246-9, 2007.

Wu, W., Liu, Y., and Betts, A. K.: Observationally based evaluation of NWP reanalyses in modeling cloud properties over the southern great plains. Journal of Geophysical Research. Atmospheres, 117(12) http://dx.doi.org/10.1029/2011JD016971, 2012.

Yuan, Jian, and Houze JR, Robert A.: Deep convective systems observed by a-train in the tropical indo-pacific region affected by the MJO. Journal of the Atmospheric Sciences, 70(2), 465–486. https://doi.org/10.1175/JAS-D-12-057.1, 2013.

Zhang, H., H. Beggs, X. H. Wang, A. E. Kiss, and C. Griffin: Seasonal patterns of SST diurnal variation over the Tropical Warm Pool region, J. Geophys. Res. Oceans, 121, 8077–8094, doi:10.1002/ 2016JC012210, 2016.

Zhang, M., Rasmussen, K. L., Meng, Z., and Huang, Y.: Impacts of coastal terrain on warm-sector heavy-rain-producing MCSs in Southern China. Monthly Weather Review, 150(3), 603-624, https://doi.org/10.1175/MWR-D-21-0190.1, 2022.

Zhao, W., Huang, Y., Siems, S., and Manton, M.: The role of clouds in coral bleaching events over the Great Barrier Reef. Geophysical Research Letters, 48, e2021GL093936. https://doi. org/10.1029/2021GL093936, 2021.

Zhao, W., Y. Huang, Steven T. Siems, and Michael J. Manton: A characterization of clouds over the Great Barrier Reef and the role of local forcing, International Journal of Climatology, 1-18. https://doi.org/ 10.1002/joc.7660, 2022.